PASJ: Publ. Astron. Soc. Japan **59**, 481–486, 2007 June 25

Near-Infrared Polarization Images of the Orion Molecular Cloud 1 South Region

Jun HASHIMOTO,[1,2] Motohide TAMURA,[1] Ryo KANDORI,[1] Nobuhiko KUSAKABE,[1] Yasushi NAKAJIMA,[1]
Shuji SATO,[3] Chie NAGASHIMA,[3] Mikio KURITA,[3] Tetsuya NAGATA,[4] Takahiro NAGAYAMA,[4] and James H. HOUGH[5]
[1]*National Astronomical Observatory, 2-21-1 Osawa, Mitaka, Tokyo 181-8588*
[2]*Department of Physics, Tokyo University of Science, 1-3 Kagurazaka, Shinjuku-ku, Tokyo 162-8601*
[3]*Department of Astrophysics, Nagoya University, Chikusa-ku, Nagoya 464-8602*
[4]*Department of Astronomy, Kyoto University, Sakyo-ku, Kyoto 606-8502*
[5]*Centre for Astrophysics Research, University of Hertfordshire, Hatfield, Herts AL10 9AB, UK*
hashmtjn@optik.mtk.nao.ac.jp

(Received 2006 July 21; accepted 2006 October 6)

Abstract

We present the polarization images in the J, H, and K_s bands of the Orion Molecular Cloud 1 South region. The polarization images clearly show at least six infrared reflection nebulae (IRNe) which are barely seen or invisible in the intensity images. Our polarization vector images also identify the illuminating sources of the nebulae; IRN 1 and 2, IRN 3, 4, and 5, and IRN 6 are illuminated by three IR sources, Source 144−351, Source 145−356, and Source 136−355, respectively. Moreover, our polarization images suggest the candidate driving sources of the optical Herbig–Haro objects for the first time; HH 529, a pair of HH 202 and HH 528 or HH 203/204, and HH 530 and HH 269 are originated from Source 144−351, Source 145−356, and Source 136−355, respectively.

Key words: dust — infrared: ISM — ISM: individual (Orion Molecular Cloud 1 South) — polarization

1. Introduction

The Orion nebula region has two luminous star-forming cloud cores which lie immediately behind the young (1 Myr) Orion nebula cluster (ONC) centered on the bright Trapezium OB stars. One is the $\sim 10^5 L_\odot$ BN/KL region in Orion molecular cloud 1 (OMC-1) and the other is the $\sim 10^4 L_\odot$ OMC-1S region. The BN/KL region has a number of compact infrared sources (IRc), of which only BN, IRc2, and IRc9 are believed to be self-luminous, and are associated with a wide-angle bipolar outflow, powerful masers, and ultracompact HII regions (see O'Dell 2001 for a recent review).

The OMC-1S region, located $\sim 100''$ south of the BN/KL complex, is a young and highly active star-formation region. This region includes a number of deeply embedded mid-IR sources (Smith et al. 2004), a luminous far-IR/submillimeter source FIR 4 (Mezger et al. 1990), a dense molecular condensation CS 3 (Mundy et al. 1986), and at least four molecular outflows (Ziurys et al. 1990; Rodríguez-Franco et al. 1999; Zapata et al. 2005, 2006). At least seven optical Herbig–Haro objects (HH 202, HH 269, HH 529, HH 203/204, HH 530, HH 625, and HH 528) originate from this region (Bally et al. 2000; O'Dell & Doi 2003). O'Dell and Doi (2003) suggested that all of the above optical Herbig–Haro objects (except HH 530 and HH 625) originate from a region only arcseconds across in the OMC-1S region, referred to as optical outflow source (OOS). However, neither IR nor radio sources are found in the OOS region. Therefore, the exciting sources of these Herbig–Haro objects remain unclear. Thus we conducted polarimetry in the J, H, and K_s bands since infrared polarization studies could indicate the illuminating/exciting sources of the infrared nebulae and the outflows (Nagata et al. 1983; Hodapp 1984; Sato et al. 1985; Tamura et al. 1991).

In this paper, we report on the discovery of several infrared reflection nebulae (IRNe). We also discuss the exciting source candidates of the optical Herbig–Haro objects in the OMC-1S region.

2. Observations and Results

Near-infrared (NIR) polarization images were obtained on 2005 December 26 with the NIR camera SIRIUS, a Simultaneous three-color InfraRed Imager for Unbiased Survey (Nagayama et al. 2003), and its polarimeter mounted on InfraRed Survey Facility (IRSF), 1.4 m telescope at the South African Astronomical Observatory in Sutherland, South Africa. The image scale of the array is $0\farcs45$ pixel^{-1}, giving a field of view of $7\farcm7 \times 7\farcm7$. The polarimeter is composed of an achromatic (1–2.5 μm) wave plate rotator and a polarizer unit which are located on the upstream side of the camera. More details are described elsewhere (Kandori et al. 2006). The polarizations were measured by stepping the half wave plate to four angular positions (0°, 45°, 22.°5, and 67.°5). Ten dithered frames were observed per wave plate position, and we observed 9 sets for the object, giving 9×10 frames of 10 s integration per wave plate position. Seeing conditions were $\sim 1\farcs5$ (FWHM) in the J band.

The data were reduced in the standard manner of infrared image reduction: subtracting a dark-frame and dividing by a flat-frame. In addition, the data for each wave plate position (I_0, I_{45}, $I_{22.5}$, and $I_{67.5}$) were registered, and then combined. Stokes I, Q, U parameters, degree of polarization (P), and position angle (θ) are calculated as follows (see, e.g., Tamura et al. 2003).

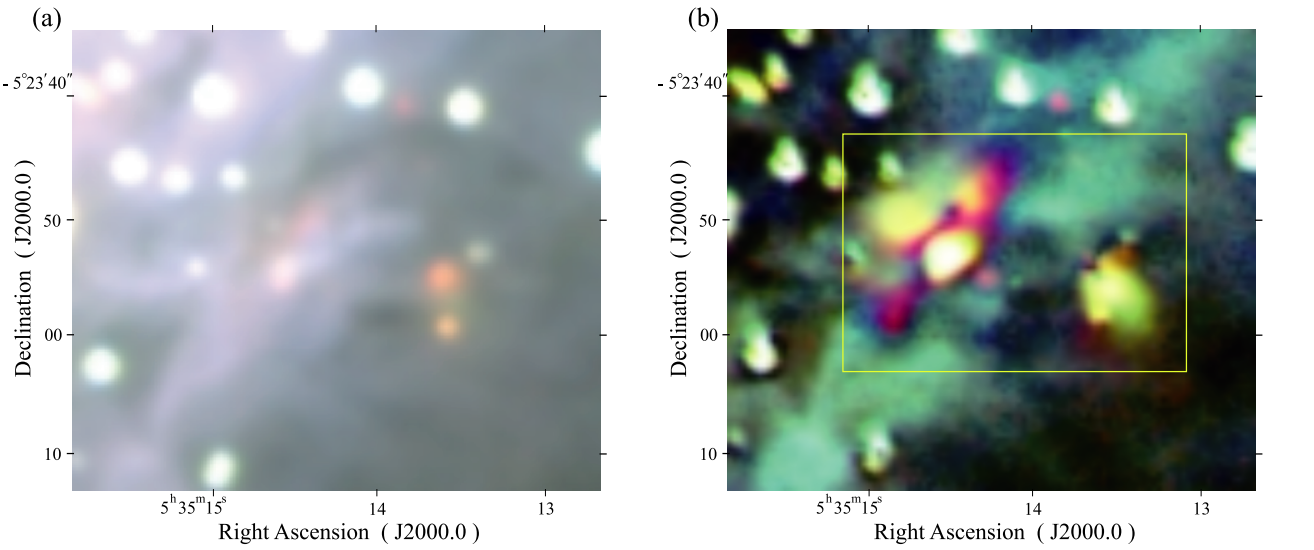

Fig. 1. Near-infrared three-color composite images of the Orion Molecular Cloud 1 South (OMC-1S) region in the J, H, and $K_{\rm s}$ bands (J: blue, H: green, $K_{\rm s}$: red). (a) and (b) show total intensity and polarized intensity images, respectively.

$$I = \{I_0 + I_{45} + I_{22.5} + I_{67.5}\} \,/\, 2, \quad (1)$$

$$Q = I_0 - I_{45},\ U = I_{22.5} - I_{67.5}, \quad (2)$$

$$P = \sqrt{\left(\frac{Q}{I}\right)^2 + \left(\frac{U}{I}\right)^2},\ \text{and}\ \theta = \frac{1}{2}\arctan\left(\frac{U}{Q}\right). \quad (3)$$

For the region of $26'' \times 20''$ of OMC-1S, the polarized intensity images, and polarization vector images in the J, H, and $K_{\rm s}$ bands obtained with the above calculations are shown in figure 1(b) and figures 2(a), (b), and (c), respectively. The entire field ($7\farcm7 \times 7\farcm7$) of the data is discussed elsewhere (Tamura et al. 2006).

3. Discussion

3.1. Illuminating Sources of the Reflection Nebulae

Figures 1(a) and (b) show how the total intensity and polarization images differ from each other. Both figures 1(a) and (b) are color-composite images in the J, H, and $K_{\rm s}$ bands (J: blue, H: green, $K_{\rm s}$: red) which are constructed with the calculations in section 2. In figure 1(b), there are several nebulae in the yellow box region, which are much more clearly seen than in figure 1(a). This is because they are obscured by a diffuse nebula in the intensity image. We identify them as IRNe and refer to them as IRN 1 to 6 as shown in figure 3.

Figures 2(a), (b), and (c) show polarization vector images superposed on the intensity image in the J, H, and $K_{\rm s}$ bands in a yellow box region of figure 1(b), respectively. In figures 2(a), (b), and (c), the polarization vectors show different centrosymmetric patterns suggesting that IRN 1 and 2, IRN 3, 4, and 5, and IRN 6 are illuminated by three independent sources. In order to identify these sources, we plotted the NIR (3.6 μm), MIR (8.8, 11.7, and 18.75 μm), and radio (CO $J = 2 \rightarrow 1$) sources in figure 2(d). We refer to these sources as marked in figure 2(d), e.g., Source 144−351. The NIR, MIR, and radio sources are detected by the Spitzer Space Telescope, Smith et al. (2004), and Zapata et al. (2005), respectively. In addition, we plotted the vectors in the $K_{\rm s}$ band rotated by 90° in figure 2(d), since the direction normal to each polarization vector indicates the source of illumination. The convergence of these lines show that Source 144−351, Source 145−356, and Source 136−355 are most likely to be the sources of illumination for IRN 1 and 2, IRN 3, 4, and 5, and IRN 6, respectively. Since diffuse radiation from the Trapezium cluster is not negligible in the J and H bands (Tamura et al. 2006), we only use the vectors in the $K_{\rm s}$ band in order to identify the source of illumination.

We consider that these IRNe correspond to the walls of the outflow material, since a close relationship has been suggested between IRN and CO bipolar outflow (Nagata et al. 1983; Hodapp 1984; Sato et al. 1985; Yamashita et al. 1989). The relationship is that these outflows are or were powerful enough to make a hollow place within their parent molecular cloud, in a direction that tends to be perpendicular to the optically thick circumstellar disk, allowing radiation from the star to escape along the polar directions, and then dust grains associated with a bipolar outflow to be scattered off. Indeed, viewed at low spatial resolution, the extension of IRN tends to be consistent with that of CO outflow.

Based on this interpretation, a suggested geometry of each outflow and associated IRN is depicted in figure 2(d); the blue and red cones mean blueshifted and redshifted outflows, respectively. IRN 6 associated with Source 136−355 has a clear monopole structure, which means that IRN 6 corresponds to a blueshifted outflow. The redshifted counterpart IRN is probably obscured and invisible. Other examples of such monopolar IRNe are R Mon (Aspin et al. 1985), Cep A (Jones et at. 2004), and GL 2591 (Minchin et al. 1991). IRN 3 and IRN 4 have a bipolar structure extending northwestward and southeastward; we suggest that IRN 3 corresponds to a blueshifted outflow and IRN 4 corresponds to a redshifted outflow. This is because IRN 3 is detected in all of the J, H, and $K_{\rm s}$ bands, while IRN 4 is only in the $K_{\rm s}$ band, which suggests a heavier extinction toward IRN 4.

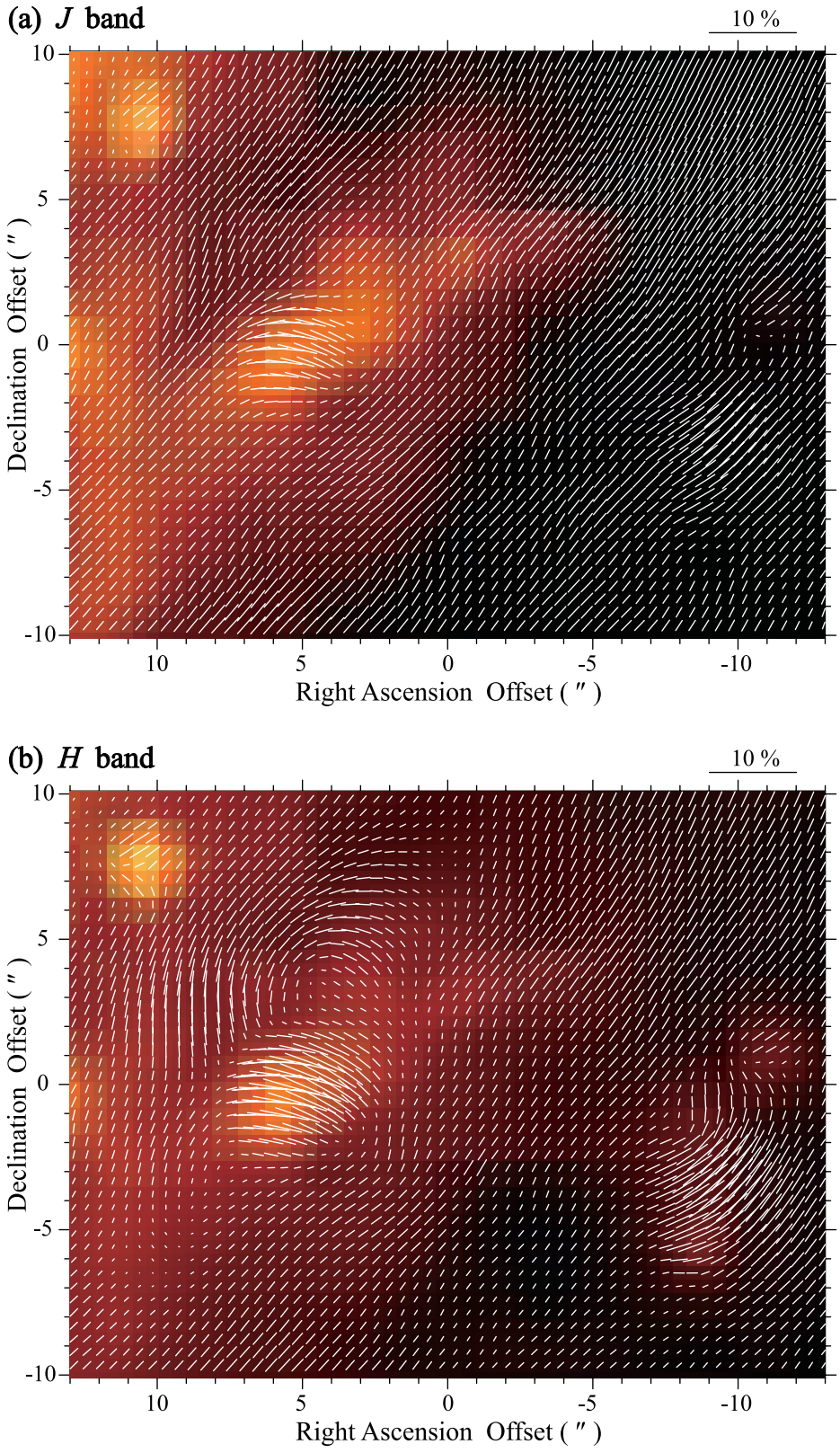

Fig. 2. (a), (b), and (c): Polarization vectors superposed on the intensity image in the J, H, and K_s bands, respectively. For these polarization vector images, the local background polarizations are not subtracted. On these scales, $3''$ represents the length of 10% polarization vector. (d): Positions of NIR, MIR, and radio sources. The polarization vectors in the K_s band are rotated 90° in order to identify the illuminating sources of IRNe. For constructing this 90° rotated vector images, the local background, which is determined at $(-10'', 10'')$, is subtracted. The polarization vectors in the low polarized intensity regions are not plotted for presentation purpose. The $(0'', 0'')$ coordinates are $5^h35^m14.^s1, -5°23'54.''2$ (J2000.0).

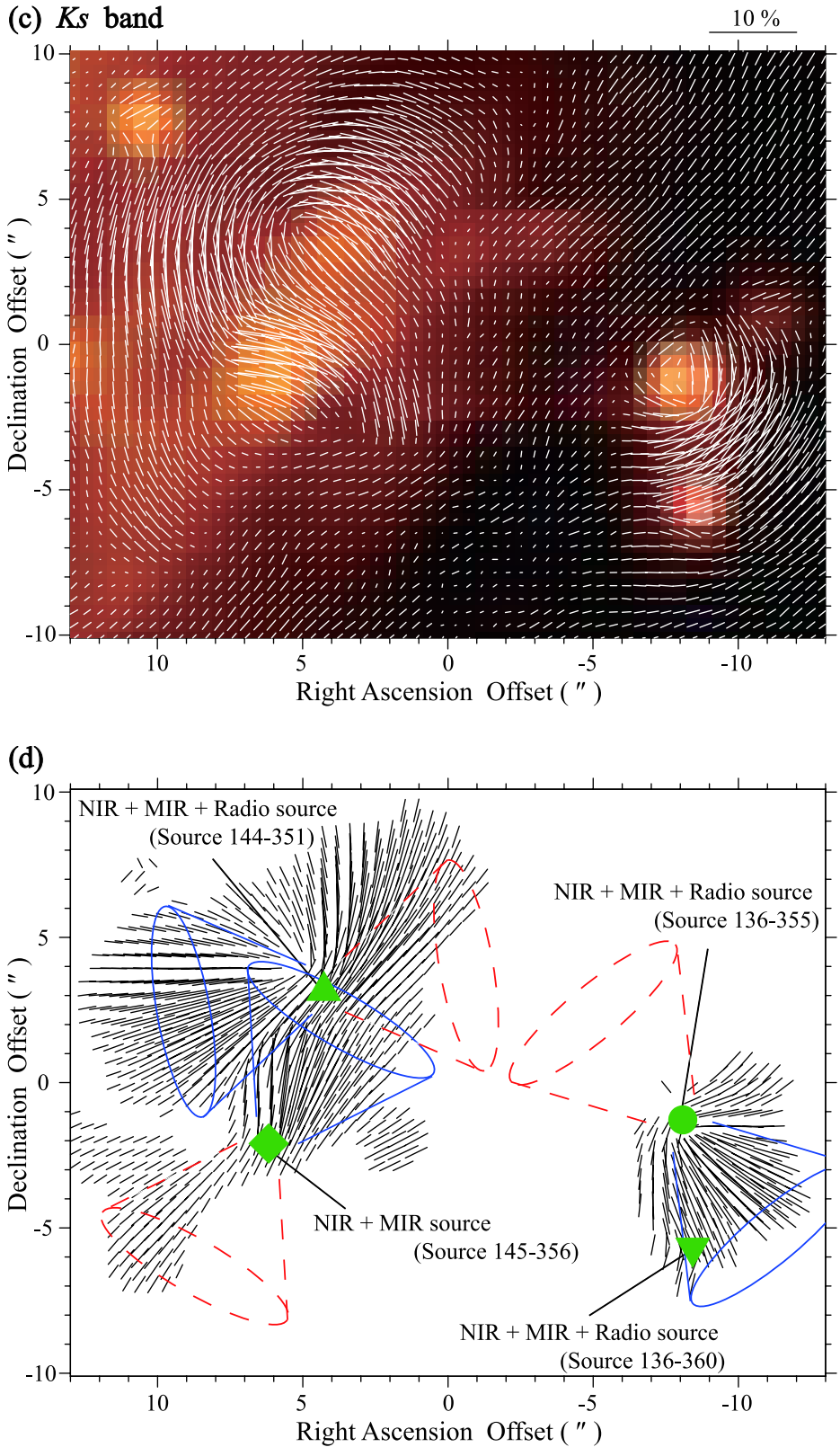

Fig. 2. (Continued.)

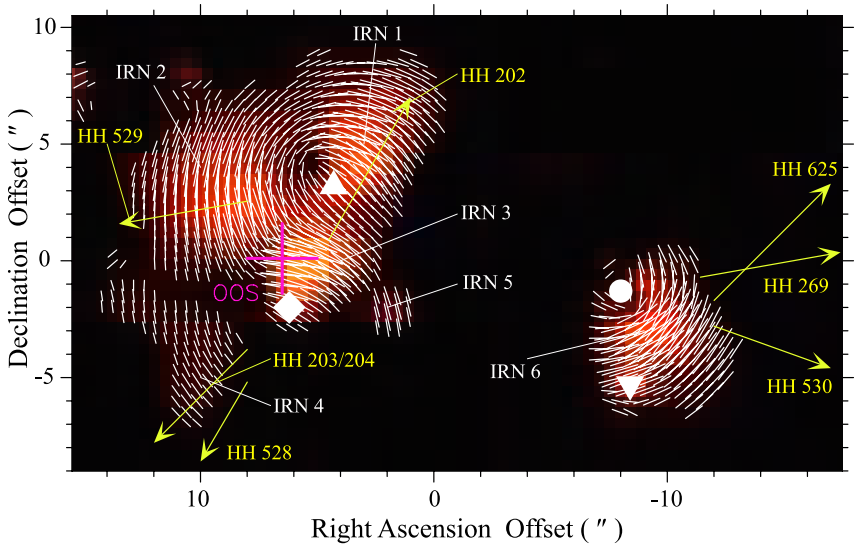

Fig. 3. The yellow arrows show the direction of the HH objects originating from the OMC-1S region. The polarization vector image superposed on polarized intensity color image in the K_s band. For these vector images, local background, which is determined at $(-10'', 10'')$, is subtracted. The polarization vectors on the low polarized intensity regions are not plotted for presentation purpose. The cross denotes the position of the OOS (O'Dell & Doi 2003). The solid symbols are the same as those of figure 2(d) and the $(0'', 0'')$ coordinates are the same as those of figure 2.

Similarly, we consider that IRN 1 and IRN 2 have a likely bipolar structure extending eastward and westward; we suggest a blueshifted outflow component in IRN 2 and a redshifted outflow component probably in IRN 1. This is because IRN 1 is redder than IRN 2 in figure 1(b). In addition, the small region of IRN 5 seems to be associated with a local high density region.

Table 1 summarizes the measured maximum degrees of polarization in IRN 1 to 6. Subtracting the local background polarization, which is determined at $(-10'', 10'')$ in figure 2, produced larger degrees of polarization in the IRNe. However, this had little effect on the geometry of the centrosymmetric polarization patterns. This is most likely to be due to the contribution of unpolarized ionized gas emission in the background diffuse radiation. Although the apparent polarization of these IRNe is small (a few %), the level of degrees of polarization after the background subtraction is comparable to that of other IRNe such as GL 2591 ($\sim 10\%$ in the K band: Minchin et al. 1991).

3.2. *Possible Exciting Sources of the Herbig–Haro Objects*

As mentioned in section 1, seven optical Herbig–Haro objects (HH 202, HH 269, HH 529, HH 203/204, HH 530, HH 625, and HH 528) originate from the OMC-1S region. Figure 3 shows the polarization vector map superposed on polarized intensity image in the K_s band, together with the directions of the HH outflows, and the optical outflow source (OOS) suggested by O'Dell and Doi (2003), marked with an error bar ($1\farcs5 \times 1\farcs5$). Here we discuss possible associations between these outflows and the embedded sources indicated in subsection 3.1, based on our polarization data and directions of IRNe.

HH 529 — HH 529 is blueshifted (Walter et al. 1995), and extended eastward from OMC-1S at PA $\sim 100°$. The direction of HH 529 corresponds approximately to the extension of IRN 2. Hence we conclude that HH 529 originates from Source 144−351.

HH 269 — HH 269 is also blueshifted (Walter et al. 1995), and extended westward at PA $\sim 280°$. Recently, Zapata et al. (2006) found a SiO bipolar outflow extended eastward and westward from Source 136−355, and concluded that the blueshifted SiO outflow at PA $\sim 280°$ could be powering HH 269. However, we found IRN 6 extended southwestward from Source 136−355. There might be another source powering HH 269 behind Source 136−355 which illuminates IRN 6.

HH 202 — HH 202 is one of the first HH objects to be recognized in the Orion Nebula (Cantó et al. 1980), and is a highly collimated jet (Rosado et al. 2001), extending at PA $\sim 330°$. This direction corresponds approximately to the extension of IRN 3. So we conclude that HH 202 originates from Source 145−356.

HH 528 and HH 203/204. — HH 528 has a low-velocity redshifted component (Smith et al. 2004) at PA $\sim 160°$ and HH 203/204 has a blueshifted component (O'Dell et al. 1997) at PA $\sim 135°$. We consider that HH 528 is most likely to be a counterpart to HH 202, since the blueshifted HH 202 should have a redshifted counterflow.

Table 1. Maximum degrees of polarization in the JHK_s bands.

IRNe	J band*	H band*	K_s band*
1	——	$\sim 2\%$ (17%)	$\sim$ 7% (27%)
2	$\sim 5\%$ (10%)	$\sim 3\%$ (10%)	$\sim$ 7% (19%)
3	——	$\sim 8\%$ (18%)	$\sim$ 9% (16%)
4	——	——	$\sim$ 3% (7%)
5	——	——	$\sim$ 4% (12%)
6	——	$\sim 8\%$ (19%)	$\sim 10\%$ (20%)

* The values in the parenthesis are after the background subtraction.

Table 2. IR sources, their associated IRNe, and Herbig–Haro objects.

IR sources	Detected wavelengths	IRNe	HH objects
Source 144−351	NIR, MIR, Radio	IRN 1, IRN 2	HH 529
Source 145−356	MIR, Radio	IRN 3, IRN 4, IRN 5	HH 202, HH 528 or HH 203/204
Source 136−355	NIR, MIR, Radio	IRN 6	HH 530, HH 269
Source 136−360	NIR, MIR, Radio	none	HH 625

HH 530 — HH 530 extending at PA $\sim 250°$ was first identified by Bally et al. (2000), where they suggested that HH 530 originated from the FIR 4/CS 3 region located $\sim 20''$ south of Source 136−355, since the highly collimated, low-velocity redshifted CO outflow from the FIR 4/CS 3 region was reported in Schmid-Burgk et al. (1990). However, HH 530 is not aligned in the direction of the measured low-velocity outflow. Hence we consider that HH 530 originates from Source 136−355 since the direction of HH 530 corresponds approximately to the extension of IRN 6.

HH 625 — HH 625 is a blueshifted HH object extending at PA $\sim 325°$ (O'Dell & Doi 2003). Zapata et al. (2005) conducted high resolution ($\sim 1''$) CO line observations, and reported a blueshifted CO outflow emanated from Source 136−360 at PA $\sim 305°$. Hence Source 136−360 is a likely source of HH 625. Unfortunately, we were unable to detect any IRNe associated with Source 136−360.

4. Conclusions

We have conducted the polarimetric imaging of OMC-1S. We found that there are at least six IRNe in this region and identified the illuminating sources of these nebulae; IRN 1 and 2, IRN 3–5, and IRN 6 are illuminated by the IR sources, Source 144−351, 145−356, and 136−355, respectively. In addition, making a comparison between the extension of IRNe and the direction of Herbig–Haro objects, we suggest the exciting source of the optical Herbig–Haro objects; HH 529, a pair of HH 202 and HH 528 or HH 203/204, and HH 530 and HH 269 are originated from Source 144−351, Source 145−356, and Source 136−355, respectively. Table 2 summarizes the illuminating sources of IRNe and the driving sources of Herbig–Haro objects. Further high spatial resolution CO observations should be undertaken for revealing the kinematics of outflows in OMC-1S.

We are very grateful to the referee, John Bally, for helpful suggestions. We also thank Robert O'Dell for useful comments. This work was partly supported by a Grant-in-Aid for Scientific Research on Priority Areas (No. 16340061) from the Ministry of Education, Culture, Sports, Science and Technology.

References

Aspin, C., McLean, I. S., & Coyne, G. V. 1985, A&A, 149, 158
Bally, J., O'Dell, C. R., & McCaughrean, M. J. 2000, AJ, 119, 2919
Cantó, J., Goudis, C., Johnson, P. G., & Meaburn, J. 1980, A&A, 85, 128
Hodapp, K.-W. 1984, A&A, 141, 255
Jones, T. J., Woodward, C. E., & Kelley, M. S. 2004, AJ, 128, 2448
Kandori, R., et al. 2006, Proc. SPIE, 6269, 626951
Mezger, P. G., Wink, J. E., & Zylka, R. 1990, A&A, 228, 95
Minchin, N. R., Hough, J. H., McCall, A., Aspin, C., Hayashi, S. S., Yamashita, T., & Burton, M. G. 1991, MNRAS, 251, 508
Mundy, L. G., Scoville, N. Z., Baath, L. B., Masson, C. R., & Woody, D. P. 1986, ApJ, 304, L51
Nagata, T., Sato, S., & Kobayashi, Y. 1983, A&A, 119, L1
Nagayama, T., et al. 2003, Proc. SPIE, 4841, 459
O'Dell, C. R. 2001, ARA&A, 39, 99
O'Dell, C. R., & Doi, T. 2003, AJ, 125, 277; Erratum 125, 2753
O'Dell, C. R., Hartigan, P., Lane, W. M., Wong, S. K., Burton, M. G., Raymond, J., & Axon, D. J. 1997, AJ, 114, 730
Rodríguez-Franco, A., Martín-Pintado, J., & Wilson, T. L. 1999, A&A, 344, L57
Rosado, M., de la Fuente, E., Arias, L., Raga, A., & Le Coarer, E. 2001, AJ, 122, 1928
Sato, S., Nagata, T., Nakajima, T., Nishida, M., Tanaka, M., & Yamashita, T. 1985, ApJ, 291, 708
Schmid-Burgk, J., Güsten, R., Mauersberger, R., Schulz, A., & Wilson, T. L. 1990, ApJ, 362, L25
Smith, N., Bally, J., Shuping, R. Y., Morris, M., & Hayward, T. L. 2004, ApJ, 610, L117
Tamura, M., et al. 2006, ApJ, 649, L29
Tamura, M., Fukagawa, M., Murakawa, K., Suto, H., Itoh, Y., & Doi, Y. 2003, Proc. SPIE, 4843, 190
Tamura, M., Gatley, I., Joyce, R. R., Ueno, M., Suto, H., & Sekiguchi, M. 1991, ApJ, 378, 611
Walter, D. K., O'Dell, C. R., Hu, X., & Dufour, R. J. 1995, PASP, 107, 686
Yamashita, T., Suzuki, H., Kaifu, N., Tamura, M., Mountain, C. M., & Moore, T. J. T. 1989, ApJ, 347, 894
Zapata, L. A., Ho, P. T. P., Rodríguez, L. F., O'Dell, C. R., Zhang, Q., & Muench, A. 2006, ApJ, 653, 398
Zapata, L. A., Rodríguez, L. F., Ho, P. T. P., Zhang, Q., Qi, C., & Kurtz, S. E. 2005, ApJ, 630, L85.
Ziurys, L. M., Wilson, T. L., & Mauersberger, R. 1990, ApJ, 356, L25